

## Studies on Fluid Dynamics of the Flow Field and Gas Transfer in Orbitally Shaken Tubes

### Li-kuan Zhu

School of Mechatronics Engineering, Harbin Institute of Technology, Harbin, Heilongjiang, People's Republic of China

Laboratory of Cellular Biotechnology (LBTC), Faculty of Life Sciences, École Polytechnique Fédérale de Lausanne (EPFL), Lausanne CH-1015 Switzerland

### Bo-yan Song

School of Mechatronics Engineering, Harbin Institute of Technology, Harbin, Heilongjiang, People's Republic of China

### Zhen-long Wang

School of Mechatronics Engineering, Harbin Institute of Technology, Harbin, Heilongjiang, People's Republic of China

### Dominique T. Monteil

Laboratory of Cellular Biotechnology (LBTC), Faculty of Life Sciences, École Polytechnique Fédérale de Lausanne (EPFL), Lausanne CH-1015 Switzerland

### Xiao Shen

Laboratory of Cellular Biotechnology (LBTC), Faculty of Life Sciences, École Polytechnique Fédérale de Lausanne (EPFL), Lausanne CH-1015 Switzerland

### David L. Hacker

Laboratory of Cellular Biotechnology (LBTC), Faculty of Life Sciences, École Polytechnique Fédérale de Lausanne (EPFL), Lausanne CH-1015 Switzerland

Protein Expression Core Facility (PECF), Faculty of Life Sciences, École Polytechnique Fédérale de Lausanne (EPFL), CH-1015 Lausanne, Switzerland

### Maria De Jesus

ExcellGene SA, Monthey CH-1870 Switzerland

### Florian M. Wurm

Laboratory of Cellular Biotechnology (LBTC), École Polytechnique Fédérale de Lausanne (EPFL), Lausanne CH-1015 Switzerland

ExcellGene SA, Monthey CH-1870 Switzerland

DOI 10.1002/btpr.2375

Published online October 31, 2016 in Wiley Online Library (wileyonlinelibrary.com)

*Orbitally shaken cylindrical bioreactors [OrbShake bioreactors (OSRs)] without an impeller or sparger are increasingly being used for the suspension cultivation of mammalian cells. Among small volume OSRs, 50-mL tubes with a ventilated cap (OSR50), originally derived from standard laboratory centrifuge tubes with a conical bottom, have found many applications including high-throughput screening for the optimization of cell cultivation conditions. To better understand the fluid dynamics and gas transfer rates at the liquid surface in OSR50, we established a three-dimensional simulation model of the unsteady liquid forms (waves) in this vessel. The studies verified that the operating conditions have a large effect on the interfacial surface. The volumetric mass transfer coefficient ( $k_L a$ ) was determined experimentally and from simulations under various working conditions. We also determined the liquid-phase mass transfer coefficient ( $k_L$ ) and the specific interfacial area ( $a$ ) under different conditions to demonstrate that the value of  $a$  affected the gas transfer rate more than did the value of  $k_L$ . High oxygen transfer rates, sufficient for supporting the high-density culture of mammalian cells, were found. Finally, the average axial velocity of the liquid was identified to be an important parameter for maintaining cells in suspension. Overall these studies provide valuable insights into the preferable operating conditions for the OSR50, such as those needed for cell cultures requiring high oxygen levels. © 2016 American Institute of Chemical Engineers *Biotechnol. Prog.*, 33:192–200, 2017*

Contract grant sponsor: China Scholarship Council (CSC) and EPFL;  
Contract grant number: 201306120128.

Correspondence concerning this article should be addressed to Z.-L. Wang at wangzl@hit.edu.cn and F. M. Wurm at florian.wurm@epfl.ch

*Keywords: CHO cells, orbitally shaken bioreactors, computational fluid dynamics, cell suspension, oxygen transfer rate*

## Introduction

Single-use cell culture technology is playing an important role in biopharmaceutical manufacturing because of the commercial availability of a wide variety of disposable bioreactors and of the need for greater flexibility in production processes.<sup>1–4</sup> Disposable orbitally shaken bioreactors (OSRs) with working volumes from small (<2 L) to large scale (<2000 L) have been used to cultivate animal cells in suspension.<sup>5–10</sup> In contrast to stirred-tank bioreactors (STRs) that require the sparging of pure oxygen into the liquid phase, it is possible with OSRs to adequately supply oxygen for high-density animal cell cultures with air only, providing the gas passively or actively into the head space over the liquid phase without a sparger. Among the small-scale bioreactors for animal cell culture, 50-mL ventilated centrifuge tubes (OSR50) have been used for the high-density cultivation of Chinese hamster ovary (CHO) cells, the predominant mammalian cell host for commercial recombinant protein production in suspension culture, as well as other mammalian and insect cells.<sup>11–13</sup>

Engineering principles such as the volumetric mass transfer coefficient ( $k_La$ ), the mixing time, and the volumetric power consumption are crucial parameters for bioprocess scale-up in all types of bioreactors.<sup>8,14–16</sup> For the OSR50, these engineering principles have not yet been fully characterized. Computational fluid dynamics (CFD) is frequently used as a tool for the modeling of the hydrodynamics and parameters of mass transfer.<sup>17</sup> For example, the volume averaged  $k_La$  of STRs can be estimated under varying process conditions using a CFD tool coupled with a population balance model (PBM).<sup>18</sup> However, the results from studies with STRs cannot be applied to OSRs. Here CFD tools were used to determine the mass transfer coefficient ( $k_L$ ) and the specific interface area ( $a$ ) in the OSR50 under a variety of conditions. By combining CFD with the cultivation of CHO cells in suspension, the correlation between fluid axial velocity ( $u_z$ ) and the cell suspension state in the OSR50 was investigated. To our knowledge this is the first study on gas and liquid interactions in the OSR50, providing valuable predictions on suitable operation conditions.

## Material and Methods

### Orbitally shaken tube

The TubeSpin® bioreactor 50 (TPP, Trasadingen, Switzerland) is modified from a standard 50-mL conical bottom centrifugation tube by substitution of the standard cap with a vented one, featuring five ventilation holes with different diameters. In this case all holes were kept open, since water loss by evaporation was minimal due to the use of an incubator shaker with a humidity setting of >80%. Sterility within the tube was assured by a gas-permeable membrane with a pore size of 0.2  $\mu\text{m}$  fixed on the inside of the cap. The tube is referred to here as the OSR50.

### Cell cultivation

Two clonal CHO-derived recombinant cell lines were used for this work. A suspension-adapted, clonal cell line

(CHODG44-IgG) producing a recombinant antibody was derived from CHO DG44 cells as previously described.<sup>19</sup> The cells were grown in ProCHO5 medium (Lonza, Verviers, Belgium) in an ISF1-X incubator shaker (Kühner AG, Basel, Switzerland) at 37°C with 5% CO<sub>2</sub> and 85% humidity. The shaking diameter was set at 50 mm for all experiments. For routine maintenance, cells were subcultivated twice per week in OSR50s at a seeding density of  $0.5 \times 10^6$  cells mL<sup>-1</sup> at a volume of 10 mL. The cell density and viability were determined with a hemocytometer using the Trypan Blue exclusion method. A second recombinant CHO cell line (CHOExpress™RP1; ExcellGene, Monthey, Switzerland) was grown in an chemically-defined proprietary medium (XLG CHO CDM; ExcellGene) under the same culture conditions as indicated above. For fed-batch cell cultivation, a commercially available feed (Hyclone Cell Boost 7a and 7b; GE Healthcare Life Sciences, Glattbrugg, Switzerland) was added daily from day 3 to day 11 post-inoculation according to the manufacture's specifications.

### Modeling of a two-phase flow

When used for cell cultivation there are two phases in the OSR50: A water-like liquid phase (typically the cell culture medium with suspended cells having a slightly higher density than water) with defined values of density, viscosity, and surface tension and a gaseous phase (head space) over the liquid. In this study, a volume of fluid (VOF) model was employed to track the free air-liquid interface between the head space and the liquid phase.<sup>20</sup> This model was used to solve the interface problem by defining a fractional volume function  $\alpha$  which specifies the fraction of a computational volume filled with liquid. The shape and position of the interface were tracked by solving the  $\alpha$  transport equation (Eq. (1)):

$$\frac{\partial \alpha}{\partial t} + \mathbf{u} \cdot \nabla \alpha = 0 \quad (1)$$

where  $\alpha = 1$  indicates a computational volume that is completely full of liquid and  $\alpha = 0$  represents a volume with no liquid (therefore  $0 < \alpha < 1$  defines the gas-liquid interface) and  $\mathbf{u}$  represents the linear velocity vector.

The continuity equation (Eq. (2)) and the momentum conservation equation (Eq. (3)) were solved as follows:

$$\frac{\partial \rho}{\partial t} + \nabla \cdot (\rho \mathbf{u}) = 0 \quad (2)$$

$$\frac{\partial (\rho \mathbf{u})}{\partial t} + \nabla \cdot (\rho \mathbf{u} \mathbf{u}) = -\nabla p + \nabla \cdot (\mu (\nabla \mathbf{u} + \nabla \mathbf{u}^T)) + \rho \cdot \mathbf{g} + \mathbf{F} \quad (3)$$

where  $p$  is the pressure. The density ( $\rho$ ) (Eq. (4)) and viscosity ( $\mu$ ) (Eq. (5)) were defined as:

$$\rho = \alpha \cdot \rho_g + (1 - \alpha) \cdot \rho_l \quad (4)$$

$$\mu = \alpha \cdot \mu_g + (1 - \alpha) \cdot \mu_l \quad (5)$$

where the subscripts  $g$  and  $l$  represent the gas and liquid phases, respectively.

$\mathbf{F}$  is the surface tension acting on the gas-liquid interface as described in Eq. 6:

$$\mathbf{F} = \sigma \kappa(x) \alpha \quad (6)$$

$$\kappa = \frac{1}{|\mathbf{n}|} [(\frac{\mathbf{n}}{|\mathbf{n}|} \cdot \nabla) |\mathbf{n}| - \nabla \cdot \mathbf{n}] \quad (7)$$

$$\mathbf{n} = \nabla \alpha \quad (8)$$

where  $\sigma$  is the surface tension coefficient,  $\kappa$  is the surface curvature, and  $\mathbf{n}$  is the unit normal vector on the interface.

### Turbulence modeling

To solve equations for the dynamics in the flow field during orbital shaking, the Re-Normalization Group k-epsilon (RNG  $\kappa$ - $\epsilon$ ) model was applied to re-normalize the Reynolds-Average Navier-Stokes equation (RANS).<sup>22</sup> The RNG  $\kappa$ - $\epsilon$  model is a suitable approach for calculating the large curvature interface being produced by the orbital shaking movement.<sup>23</sup>

$$\frac{\partial(\rho k)}{\partial t} + \nabla \cdot (\rho \mathbf{u} k) = \nabla \cdot [(\alpha_k \mu_{\text{eff}} \nabla k)] + G_k - \rho \epsilon \quad (9)$$

$$\frac{\partial(\rho \epsilon)}{\partial t} + \nabla \cdot (\rho \mathbf{u} \epsilon) = \nabla \cdot [(\alpha_\epsilon \mu_{\text{eff}} \nabla \epsilon)] + C_{1\epsilon} \frac{\epsilon}{k} G_k - C_{2\epsilon} \rho \frac{\epsilon^2}{k} - R_\epsilon \quad (10)$$

where  $k$  and  $\epsilon$  are turbulent kinetic energy and turbulent dissipation rate, respectively,  $C_{1\epsilon} = 1.42$  and  $C_{2\epsilon} = 1.68$  are constants,  $\alpha_k$  and  $\alpha_\epsilon$  are the inverse effective Prandtl numbers for  $k$  and  $\epsilon$ , respectively, and both values are  $\sim 1.393$ .  $\mu_{\text{eff}}$  is the effective viscosity as defined in Eq. (11):

$$\mu_{\text{eff}} = \rho C_\mu \frac{k^2}{\epsilon} \quad (11)$$

where the constant  $C_\mu = 0.0845$ , and  $G_k$  represents the production of turbulence kinetic energy and was calculated by Eq. (12).  $R_\epsilon$  is defined in Eqs. (13) and (14).

$$G_k = \mu_t ((\nabla \bar{\mathbf{u}} + (\nabla \bar{\mathbf{u}})^T))^2 \quad (12)$$

$$R_\epsilon = \frac{C_\mu \rho \cdot \eta^3 (1 - \frac{\eta}{\eta_0}) \epsilon^2}{1 + \beta \eta^3} \frac{1}{k}, \eta_0 = 4.38, \beta = 0.012 \quad (13)$$

$$\eta = \frac{(\nabla \bar{\mathbf{u}} + (\nabla \bar{\mathbf{u}})^T) k}{\epsilon} \quad (14)$$

### Modeling of the orbital shaking movement

The orbital shaking movement was synthesized by the superposition of two individual movements<sup>24</sup>: the first was the rotation with respect to the shaking diameter and the second was the rotation around the center of the OSR50. The absolute value of the two angular velocities was the same to keep the OSR50's spatial orientation in a specific direction. This movement was modeled using a centrifugal force as a source term in the Navier-Stokes equation of the liquid in the OSR50. The centrifugal force was as follows:

$$F_x = \omega^2 R_s \cdot \cos(\omega \cdot t) \quad (15)$$

$$F_y = \omega^2 R_s \cdot \sin(\omega \cdot t) \quad (16)$$

where  $R_s$  is the shaking radius,  $F_x$  and  $F_y$  are the centrifugal force components in the x and y directions, respectively,  $\omega$  is the angular shaking velocity, and  $t$  is the time.

### Simulation conditions

Considering that large body forces (e.g., gravity and surface tension forces) exist in multiphase flows, the implicit body force treatment was used for a more robust solution to achieve convergence. The pressure-implicit with splitting of operators (PISO) scheme was employed to couple the pressure and velocity in the control volume. No slip-wall boundary conditions were applied for any boundaries of the domain. For the transient simulation, the iteration process was sensitive to the time step size. Normally, the size ( $\Delta t$ ) was determined as follows (Eq. 17):

$$\Delta t \leq \frac{\Delta L_{\text{min}}}{\mathbf{u}_{\text{max}}} \quad (17)$$

where  $\Delta L_{\text{min}} \approx 0.00172$  m is the minimum grid size and  $\mathbf{u}_{\text{max}} \approx 0.471$  m/s is the maximum linear velocity of the OSR50s. Using Eq. (17), the time step  $\Delta t$  was expected to be smaller than 0.00365 s. To guarantee the convergence of iterations, a small time step size (about 0.0000001 s) was adopted at the beginning and then steadily increased to 0.0001 s. The solver processed at least 10 s of run time to ensure that the liquid phase arrived at a steady state ( $\sim 30$  cycles at 180 rpm). All of the calculations were executed on a 8G RAM 6 processor Dell workstation (Dell, Round Rock, TX, USA) using the CFD software package FLUENT in ANSYS 15.0 (ANSYS Inc, Canonsburg, PA, USA). For each simulation case, a convergence criteria of  $\sim 1 \times 10^{-3}$  was used to decide whether to iterate or not within one time step. The mesh structure was generated using Trellis CFD meshing software (Trellis 15, Csimsoft, American Fork, UT). The mesh size of the three dimensional structure was tested at three different sizes in order to improve the computing. Three different sizes of unstructured grid were used in the simulations of OSR50 with a 10-mL filling volume at a shaking speed of 180 rpm. It was found that the grid size of  $1.0 \times 10^5$  was sufficient to generate stable simulation results (Table 1).

### Prediction of $k_L a$

The oxygen transfer rate (OTR) is an important engineering parameter for cell culture that is directly linked to  $k_L a$ , a product of the mass transfer coefficient ( $k_L$ ) and the specific interfacial area ( $a$ ). The latter can be determined using:

$$a = \frac{A}{V_L} = \frac{\text{surface area}}{\text{liquid volume}} \quad (18)$$

According to Higbie's penetration theory, which is widely accepted for gas-liquid transfer descriptions,<sup>25</sup> the mass transfer coefficient for a moving gas bubble in a liquid can be obtained by Eq. (19):

$$k_L = \frac{2}{\sqrt{\pi}} \sqrt{\frac{D_L}{t_c}} \quad (19)$$

where  $D_L$  is the diffusion coefficient of gas in the liquid and  $t_c$  is the contact or exposure time for mass transfer. Danckwerts improved this model and proposed the surface renewal theory for estimating  $k_L$  on the liquid side of a gas-liquid interface<sup>26</sup> Eq. (20):

$$k_L = \sqrt{D_L \cdot s} \quad (20)$$

where  $s$  is the surface renewal rate.

**Table 1. Grid Independence Data**

Case	Grid Size	Average Axial Velocity (m s <sup>-1</sup> )	Average Radical Velocity (m s <sup>-1</sup> )
1	1.0 × 10 <sup>5</sup>	0.0726	0.0247
2	5.0 × 10 <sup>5</sup>	0.0763	0.0283
3	1.0 × 10 <sup>6</sup>	0.0782	0.0297

Based on the surface renewal model, the eddy number distribution for isotropic turbulent flows has been derived, and an equation for predicting  $k_L$  was obtained (Eq. (21)). This equation has been applied to the calculation of the  $k_L$  value in shake flasks.<sup>27</sup>

$$k_L = K \cdot \sqrt{D_L} \left(\frac{\varepsilon}{\nu}\right)^{\frac{1}{4}} \quad (21)$$

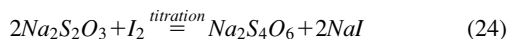
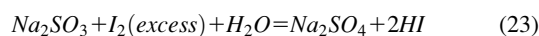
where  $\nu$  is the kinematic viscosity of liquid,  $\varepsilon$  is the energy dissipation rate, and  $K = 0.4$  is the model constant.

### Experimental method of determining $k_L a$

The sodium sulfite oxidation method was used to determine  $k_L a$  values as previously described.<sup>28–30</sup> The method is based on the reaction of sodium sulfite, a reducing agent, with dissolved oxygen in the presence of a catalyst, usually a divalent cation such as  $\text{Cu}^{2+}$  or  $\text{Co}^{2+}$ , to produce sulfate. The concentration of sodium sulfite ( $\text{Na}_2\text{SO}_3$ , Tianjin Dingshengxin Chemical Industry, Tianjin, China) in each tube was kept higher than 0.04 M to guarantee that the oxygen concentration in the liquid was zero.<sup>14</sup> The experimental conditions were kept the same as the CHO culture condition described above. For each operating condition (filling volume and shaking speed), five OSR50 tubes were run in parallel to eliminate the influence of sampling on the measurement of  $k_L a$ . Every 10 min, a sample of 2 mL was removed from each tube and mixed with 8 mL of 0.0384 M  $\text{I}_2$  (Tianjin Fengchuan Chemical Industry). The mixture was titrated with 0.1 M sodium thiosulfate ( $\text{Na}_2\text{S}_2\text{O}_3$ , Tianjin Dingshengxin Chemical Industry). When the solution became pale yellow in color, 1 mL of 1% starch solution (Tianjin Zhiyuan Chemical Industry) was added and the solution immediately turned a blue color. Drops of 0.1 M sodium thiosulfate were added until the blue color disappeared. This was considered the titration end-point. The amount of sodium sulfite remaining in the liquid was determined by Eq. (22), based on the stoichiometric coefficients in Eqs. (23) and (24). Finally, the rate of oxygen transfer was calculated with Eq. (25) and the  $k_L a$  was calculated from Eq. (22):

$$C_{\text{Na}_2\text{SO}_3}(\text{final}) = \frac{8\text{mL} \cdot C_{\text{I}_2} - 2 \cdot V_L \cdot C_{\text{Na}_2\text{S}_2\text{O}_3}}{2\text{mL}} \quad (22)$$

where  $C_{\text{Na}_2\text{SO}_3}(\text{final})$  is the concentration of the  $\text{Na}_2\text{SO}_3$  remaining in solution,  $C_{\text{I}_2}$  is the concentration of  $\text{I}_2$  (0.0384 M),  $C_{\text{Na}_2\text{S}_2\text{O}_3}$  is the concentration of  $\text{Na}_2\text{S}_2\text{O}_3$  (0.1 M), and  $V_L$  is the volume (mL) of 0.1 M  $\text{Na}_2\text{S}_2\text{O}_3$  added for titration.



$$-2 \frac{(C_{\text{Na}_2\text{SO}_3}(\text{initial}) - C_{\text{Na}_2\text{SO}_3}(\text{final}))}{dt} = \frac{dO_2}{dt} = k_L a C^* \quad (25)$$

where  $C_{\text{Na}_2\text{SO}_3}(\text{initial})$  is the initial concentration of  $\text{Na}_2\text{SO}_3$  (0.2 M) and  $C^*$  is the oxygen saturation concentration in the bulk liquid.

## Results and Discussion

### Liquid wave shape in the OSR50

While the simulated OSR50 was in orbital motion, the shape of the liquid rotating along the wall at the air–liquid interface was uniform and smooth (Figure 1). The shape of the liquid can be described as a single-crested, symmetric wave that remained unchanged from the time that the shaking speed reached a set value. A similar finding was made for the air–liquid interface in an unbaffled Erlenmeyer-type flask.<sup>31</sup> It should be mentioned that in cylindrical vessels with geometries different from that of the OSR50, we observed other wave types, including double, triple, and quadruple waves.<sup>32</sup> However, the simple, single-crested wave with its uniform interfacial area ( $A$ ) seen in our simulation of the OSR50 was helpful in the evaluation of the specific interfacial area ( $a$ ). The  $A$  of the liquid wave at an agitation speed of 180 rpm was 10.3 cm<sup>2</sup>, about 50% greater than that of the liquid column at static state (7.0 cm<sup>2</sup>) (Figures 1A,B). Likewise, the  $a$  value at 180 rpm was about 50% greater than that of the static state (Figures 1A,B). Accordingly, the wave height ( $H$ ), which is the distance between the crest and the lowest point of the gas–liquid interface, increased from 0 mm to 31.0 mm (Figures 1A,B).

The velocity field is a fundamental fluid dynamics parameter which provides basic information of the flow field. The velocity vector profile in a central vertical section of the OSR50 is shown in Figure 1C. The magnitude of velocity vector was larger near the gas–liquid interface than it was near the bottom and along the wall of the tube. Generally, the direction of the velocity vector was negative on the left side and positive on the right side of the vertical section. The magnitude of the velocity vector in the axial direction ( $\mathbf{u}_z$ ) was responsible for upward and downward liquid movement on which the interfacial area ( $A$ ) and particle suspension within the liquid phase depended.

To investigate the effect of the shaking speed and filling volume on the liquid wave, various filling volumes (10 to 50 mL) were modeled at a single shaking speed (180 rpm). In addition, a single filling volume (20 mL) was modeled at various shaking speeds (90 to 300 rpm). At a constant shaking speed of 180 rpm,  $H$  remained nearly constant as the filling volume increased from 10 to 40 mL (Figure 2A, Table 2). At a filling volume of 50 mL, the value of  $H$  decreased to 29.9 mm as the air–liquid interface came into contact with the cap of the container (Figure 2A, Table 2). The  $A$  was relatively constant at filling volumes of 20 to 40 mL, matching previous results from experiments performed in unbaffled shake flasks.<sup>24</sup> However, lower  $A$  values were observed at filling volumes of 10 and 50 mL (Table 2) as the margin of the air–liquid interface touched the conical bottom or the cap, respectively (Figure 2A). At a constant filling volume of 20 mL, the shaking speed significantly influenced the liquid wave behavior (Figure 2B). Both  $A$  and  $H$  increased with the shaking speed (Table 3).

The Froude number ( $Fr$ ), which is the ratio of centrifugal force to gravitational force, is the main driving force of the orbital shaking movement in OSRs,<sup>32</sup> and is defined in Eq. (26):

$$Fr = N^2 \cdot d / g \quad (26)$$

where  $N$  represents the shaking speed,  $g$  represents the gravitational force, and  $d$  represents the vessel diameter. For

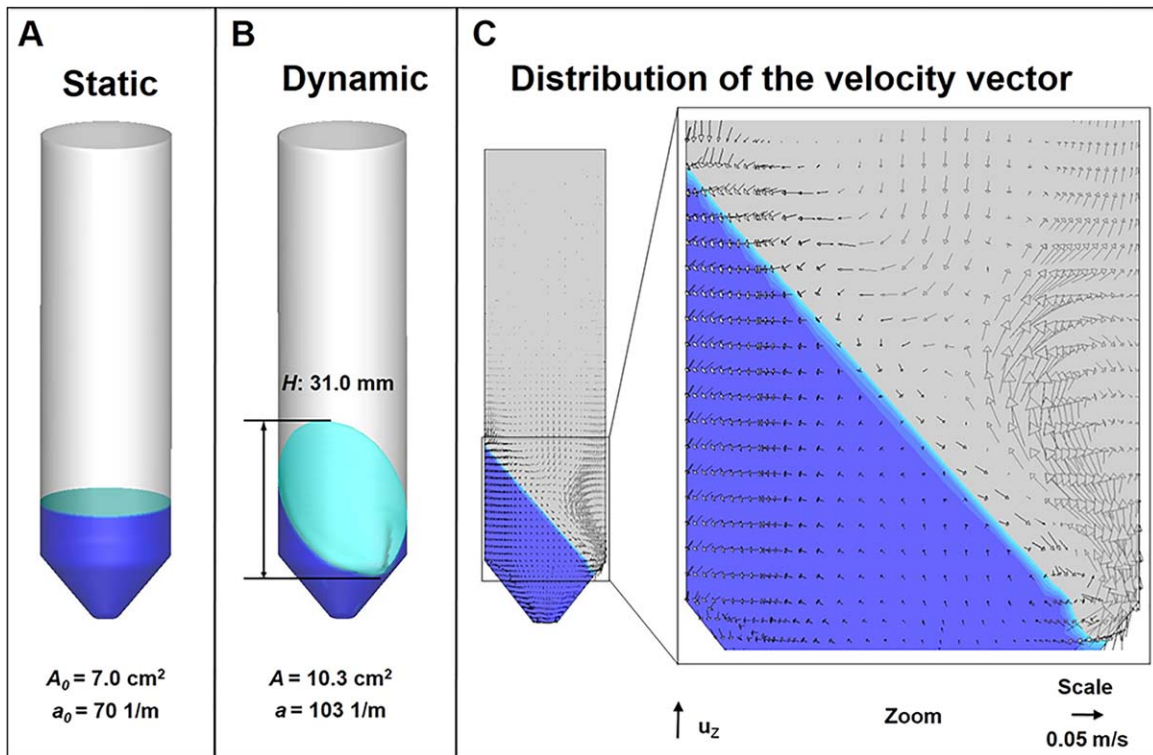


**Figure 1.** Liquid wave and velocity simulation in the OSR50 under static and dynamic conditions.

(A) Schematic diagram of the static state of the OSR50 with a filling volume of 10 mL. (B) The liquid wave of the OSR 50 under the dynamic condition. White represents the air phase while blue and green represent the liquid phase and the air–liquid interface, respectively. To visualize the air–liquid interfacial area and the velocity distribution under dynamic conditions, a simulation with a filling volume of 10 mL and a shaking speed of 180 rpm was used. The simulation was performed until the shape of the air–liquid interface remained unchanged. (C) The fundamental information of the velocity vector in the central vertical section of the OSR50 is represented. To show the liquid velocity vector more clearly, an enlarged view is provided. The velocity component in the axial direction ( $u_z$ ) is shown.

bioreactors having a fixed diameter and operated at a fixed shaking speed,  $Fr$  is constant. This may be one reason why the  $A$  and  $H$  remained similar when different filling volumes were modeled at a single shaking speed (Table 2). In contrast, an increase in shaking speed at a fixed vessel diameter will increase  $Fr$ . This may explain why both  $A$  and  $H$  increased as the shaking speed increased at a constant filling volume (Table 3).

#### Analysis of $k_L a$

Experiments in our group revealed that the OSR50 supported the cultivation of mammalian cells at high cell densities ( $>2 \times 10^7$  cells  $\text{mL}^{-1}$ , data not shown), suggesting that high gas transfer rates can be provided under certain operating conditions. To determine the  $k_L a$  for the OSR50, the  $\varepsilon$  and  $k_L$  were calculated separately. The turbulence character  $\varepsilon$  was calculated for the experiments shown in Figure 2. As the filling volume increased while the shaking speed was kept constant, the value of  $\varepsilon$  remained relatively constant (Table 2). When the filling volume was constant and the shaking speed was increased from 90 to 300 rpm, the value of  $\varepsilon$  increased (Table 3). Turbulent properties of the flow are mainly dependent on the  $Re$  number, which is defined by Eq. (27)

$$Re = \frac{\rho N d^2}{\mu} \quad (27)$$

where  $\mu$  is the molecular viscosity of the liquid as previously described for OSRs.<sup>33</sup> Thus, the shaking speed was expected

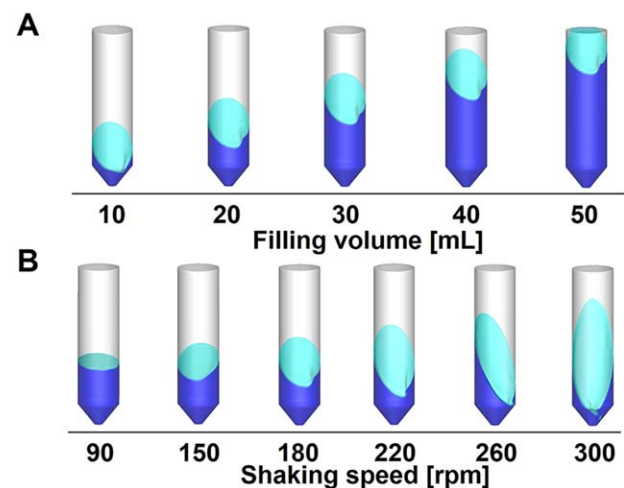


**Figure 2.** Liquid wave simulation in the OSR50 at different filling volumes and shaking speeds.

The colors of the gas and liquid phases along with the air–liquid interface are the same as in Figure 1. (A) Simulations with different filling volumes at a shaking speed of 180 rpm are shown. (B) Simulations with different shaking speeds at a filling volume of 20 mL are shown. All simulations were performed until the air–liquid interface shape remained unchanged.

to have a positive effect on the value of  $\varepsilon$ . Indeed, this was verified in our model.  $\varepsilon$  was sensitive to shaking speed (Table 3) but not to the filling volume (Table 2).

**Table 2. Simulated Wave Pattern Properties of the OSR50 at Different Filling Volumes\***

Filling Volume (mL)	Wave Height (mm)	Interface Area (cm <sup>2</sup> )	Energy Dissipation Rate (m <sup>2</sup> s <sup>-3</sup> )
10	31.0	10.3	0.0149
20	31.5	10.4	0.0145
30	31.7	10.4	0.0163
40	31.8	10.4	0.0163
50	29.9	9.94	0.0161

\*The shaking speed was maintained at 180 rpm for all filling volumes.

**Table 3. Simulated Wave Pattern Properties of the OSR50 at Different Shaking Speeds\***

Shaking Speeds (rpm)	Wave Height (mm)	Interface Area (cm <sup>2</sup> )	Energy Dissipation Rate (m <sup>2</sup> s <sup>-3</sup> )
90	7.4	7.3	0.00604
150	22.3	8.7	0.00765
180	31.5	10.4	0.0146
220	46.8	13.6	0.0288
260	63.6	17.5	0.0536
300	80.6	21.2	0.0724

\*The filling volume was maintained at 20 mL for all shaking speeds.

Under a constant shaking speed the value of the specific interface area  $a$  was found to be reduced from 103 1/m to 52 1/m when the filling volume changed from 10 to 20 mL (Figure 3A). As the filling volume increased from 20 to 50 mL,  $a$  decreased from 52 to 20 1/m, but  $k_L$  remained relatively constant (about 0.7 m h<sup>-1</sup>) as the filling volume increased from 10 to 50 mL (Figure 3A). The results indicated that it is possible to enhance the mass transfer capability of the OSR50 by using smaller filling volumes.

Next, different shaking speeds ranging from 90 rpm to 300 rpm were used to investigate the influence of this parameter on  $k_L a$  at a constant filling volume of 20 mL. Both  $k_L$  and the specific interface area  $a$  increased as the shaking speed increased (Figure 3B). Correspondingly, the  $k_L a$  increased from 20 to 111.0 1/h over this range of shaking speeds (Figure 3B). This meant that increasing the shaking speed was an effective approach to enhancing the mass transfer, as the shaking speed had a positive effect both on  $a$  and  $k_L$  (Figure 3B). When the shaking speed was kept constant, it was evident that  $k_L a$  was more dependent on  $a$  than on  $k_L$  (Figure 3A), which indicated that  $a$  plays an important role in gas transfer in the OSR50 at a given shaking speed. However,  $a$  and  $k_L$  appeared to contribute equally to  $k_L a$  for a given filling volume agitated at different shaking speeds, as the results in Figure 3B demonstrated.

For all the conditions described in Figure 3, the experimental  $k_L a$  values were determined by the sodium sulfite oxidation method. The simulated and experimental  $k_L a$  values were plotted in Figure 4. Generally, the experimental  $k_L a$  values were higher than the simulated ones (Figure 4), but the difference was not more than 20% for any condition. We believe that the difference between experimental and simulated values was caused by the reaction of oxygen with sodium sulfite during experimental operations such as sampling and titrating, resulting in an apparent increase in  $k_L a$  relative to the calculated value.

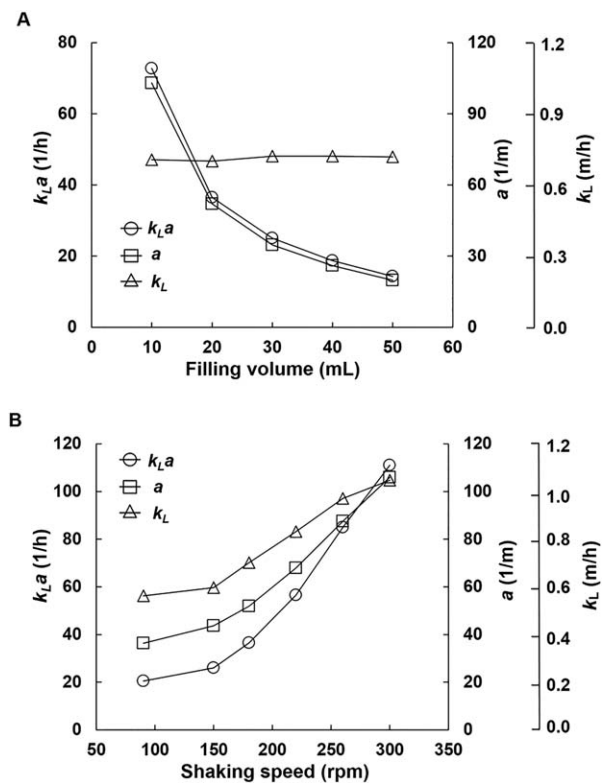


**Figure 3. Effect of filling volume and shaking speed on  $k_L a$ ,  $k_L$ , and  $a$ .**

The  $k_L a$ ,  $k_L$ , and  $a$  were determined from simulations either (A) at various filling volumes as indicated with a constant shaking speed of 180 rpm or (B) at various shaking speeds as indicated with a constant filling volume of 20 mL.

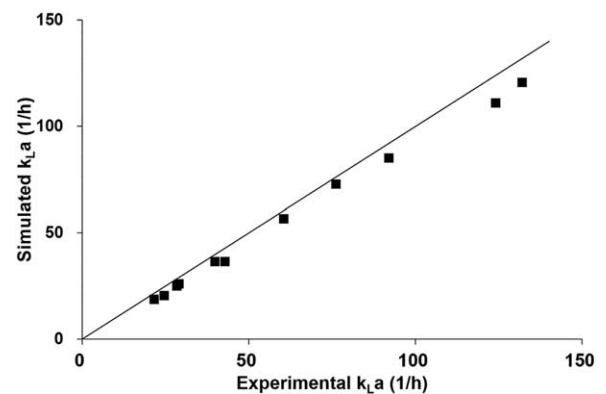


**Figure 4. Correlation between simulated and experimental  $k_L a$  values in the OSR50.**

The simulated  $k_L a$  values were taken from Figure 3. The experimental  $k_L a$  values were determined by the sodium sulfite oxidation method in an OSR50 under the same conditions as each simulation described in Figure 3. Each point on the graph represents the comparison of simulated and experimental  $k_L a$  values for each cultivation condition tested. The diagonal line represents the position of equal simulated and experimental  $k_L a$  values for any condition.

**Suspension cell culture in the OSR50**

The calculated  $k_L a$  values of the OSR50 were found to be surprisingly high under certain conditions for a non-baffled container (Figure 3). The  $k_L a$  was 72.8 1/h at a shaking speed of 180 rpm and a filling volume of 10 mL (Figure 3A). From a cell growth perspective, the higher the cell

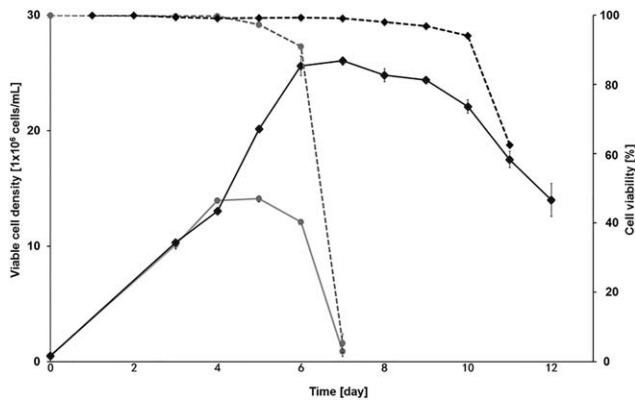


**Figure 5.** Cell growth kinetics of CHOExpress™RP1 in the OSR50 under batch and fed-batch culture conditions.

For the batch (gray lines) and fed-batch cultures (black lines), the cell density (solid lines) and cell viability (stippled lines) were measured at the times indicated. The shaking speed (180 rpm) and the filling volume (10 mL) were kept the same in the two cultures to obtain the same  $k_L a$  value for each.

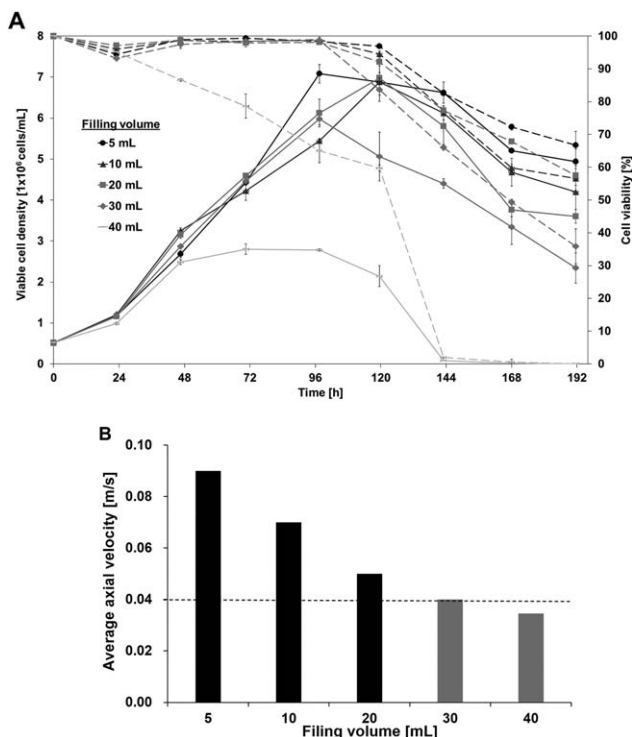


**Figure 6.** Cell cultivation and CFD simulations in the OSR50 at different filling volumes.

(A) CHO-IgG cells were cultivated in different volumes as indicated in OSR50s at a shaking speed of 180 rpm. Cultures were inoculated at  $0.5 \times 10^6$  cells  $\text{mL}^{-1}$ . The cell density (solid lines) and viability (dashed lines) were determined by the Trypan blue exclusion method at various times post-inoculation as indicated. Each experiment was performed in duplicate. (B) CFD simulations were performed with OSR50s having different filling volumes as indicated. Agitation was at 180 rpm. The average axial velocity ( $\bar{u}_z$ ) at different filling volumes was calculated. The dotted line represents a  $\bar{u}_z$  value of  $0.04 \text{ m s}^{-1}$ .

density, the more oxygen needs to be supplied to the culture. Therefore, a relatively high  $k_L a$  value is required in order to achieve this. To check whether the  $k_L a$  of the OSR50 was sufficient for supporting very high cell density cultures, an

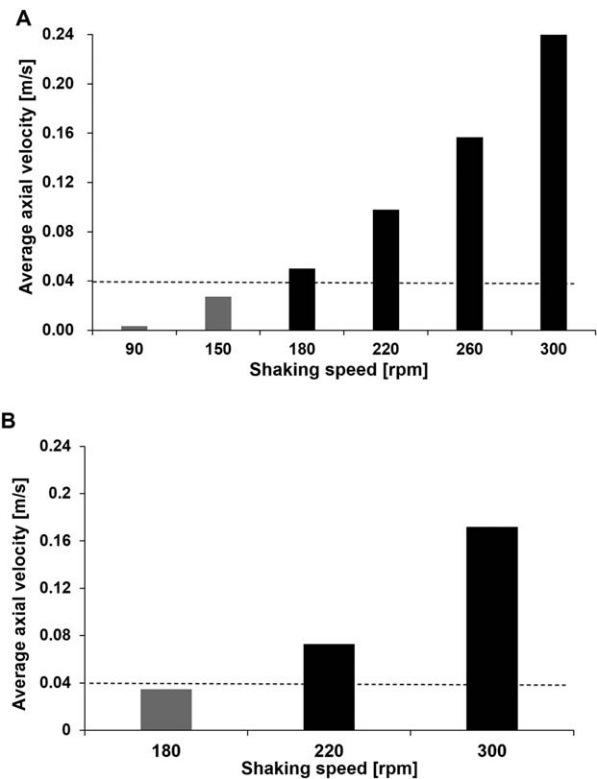


**Figure 7.** CFD simulations in the OSR50 at different shaking speeds and filling volumes.

The  $\bar{u}_z$  was calculated at filling volumes of (A) 20 mL and (B) 40 mL over a range of shaking speeds as indicated. The horizontal dotted line represents the  $\bar{u}_z$  value of  $0.04 \text{ m s}^{-1}$ .

antibody-producing CHO cell line (CHOExpress™RP1) was cultured at a shaking speed of 180 rpm with a filling volume of 10 mL under batch and fed-batch conditions using a proprietary medium developed for this cell line prior to the present work. Maximum cell densities of about  $12 \times 10^6$  cells/mL and  $24 \times 10^6$  cells/mL were found under batch and fed-batch culture conditions, respectively (Figure 5). Even higher cell densities (up to  $30 \times 10^6$  cells/mL) have been seen in the laboratories of the authors on many occasions when applying further enriched media and feeds with a diversity of clonal and non-clonal CHO cell lines (data not shown). Thus, the high  $k_L a$  of the OSR50 appeared to be a favorable factor to support the high cell densities we observed under certain conditions.

In separate experiments, another clonal cell line (CHO-IgG) was cultured in OSR50s over a range of filling volumes from 5 mL to 40 mL with a fixed shaking speed of 180 rpm. The cell growth and viability were found to be very similar for the cultures with filling volumes of 5, 10, and 20 mL but the results differed at volumes of 30 and 40 mL (Figure 6A). Some cell sedimentation was observed for the 30-mL culture, while cell sedimentation was more pronounced for the 40-mL culture. These results can explain, at least in part, the reduced cell growth at these two filling volumes.

Forces of gravity, buoyancy, inertia (caused by velocity), and adhesion (cell-cell interaction) act on mammalian cells in suspension.<sup>34,35</sup> Gravity and adhesion are resistance forces, whereas buoyancy (depending on the liquid density) and inertia are driving forces. Because the axial velocity (Figure 1C) is the most important factor to be considered for

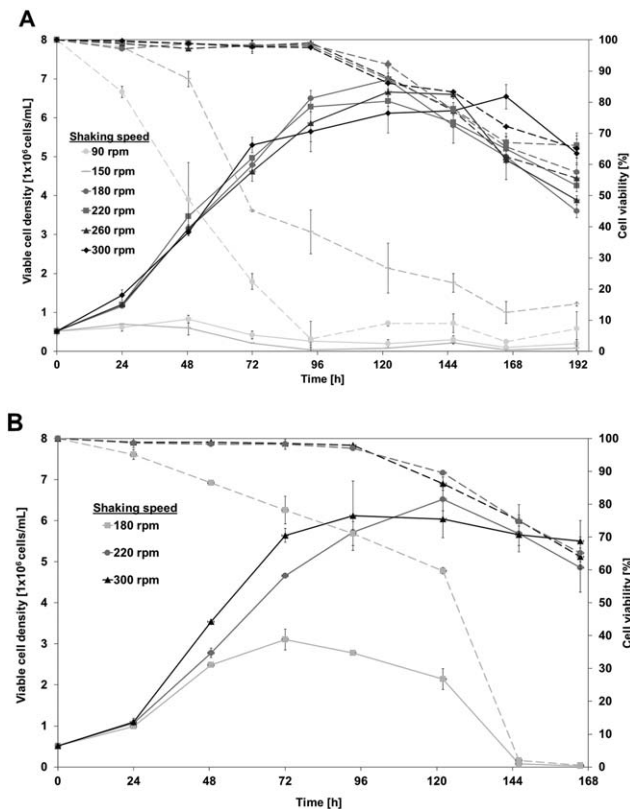


**Figure 8. Cell growth in the OSR50 at different filling volumes and shaking speeds.**

Cells were inoculated at  $0.5 \times 10^6$  cells  $\text{mL}^{-1}$  in OSR50s at filling volumes of (A) 20 and (B) 40 mL and agitated at various shaking speeds as indicated. The viable cell density (solid lines) and viability (dashed lines) were determined at various times post-inoculation as indicated. Each experiment was performed in duplicate.

inertia, the average axial-velocity  $\bar{u}_z$  of the whole liquid field was studied within cylindrical coordinates for filling volumes from 5 to 40 mL at a shaking speed of 180 rpm. Values of  $0.04 \text{ m s}^{-1}$  or lower were found at filling volumes of 30 and 40 mL (Figure 6B), the two conditions in which cell sedimentation was seen (Figure 6A). We concluded that a  $\bar{u}_z$  value greater than  $0.04 \text{ m s}^{-1}$  is necessary to maintain mammalian cells in suspension in the OSR50. Subsequently, CFD simulations at filling volumes of both 20 and 40 mL and at various shaking speeds were performed. At a filling volume of 20 mL,  $\bar{u}_z$  increased with shaking speed, but it was below  $0.04 \text{ m s}^{-1}$  at shaking speeds of 90 and 150 rpm (Figure 7A). At a filling volume of 40 mL, an  $\bar{u}_z$  value  $>0.04 \text{ m s}^{-1}$  was obtained at shaking speeds of 220 and 300 rpm but not at 180 rpm (Figure 7B). Thus, we expected cell sedimentation under cultivation conditions in which  $\bar{u}_z$  was  $0.04 \text{ m s}^{-1}$  or less.

To check the validity of the prediction, CHO-IgG cells were grown in OSR50s at either 20 or 40 mL and agitated at various shaking speeds. At a filling volume of 20 mL, cells were able to grow to a maximum cell density of  $7 \times 10^6$  cells  $\text{mL}^{-1}$  at shaking speeds of 180 rpm or more, but little or no cell growth was observed in cultures which were agitated at 90 or 150 rpm (Figure 8A). Furthermore, the cell viability of cultures shaken at 90 or 150 rpm decreased rapidly after inoculation (Figure 8A), and cell sedimentation was observed (data not shown). For a filling volume of 40 mL, cells grew to a maximal cell density of  $6\text{--}7 \times 10^6$

cells  $\text{mL}^{-1}$  at shaking speeds of 220 and 300 rpm (Figure 8B). At 180 rpm, the maximum cell density was only  $3 \times 10^6$  cells  $\text{mL}^{-1}$  (Figure 8B), and cell sedimentation was observed (data not shown). Thus, the results from the cell culture experiments validated our predictions from the CFD simulations.

## Conclusions

Using CFD and cell culture experiments, we investigated the characteristics of flow fields in the OSR50 tubes at different filling volumes and shaking speeds. The  $A$  and  $H$  of the liquid waves were found to be dependent on the shaking speed rather than the filling volume. For the  $k_L a$ , the specific interface value  $a$  was found to be more important for oxygen transfer than was the  $k_L$  value. Thus, increasing the shaking speed was found to be an effective way to enhance the oxygen supply in the OSR50. We also found a crucial parameter  $\bar{u}_z$  to predict the shaking speed necessary to maintain cells in suspension at any filling volume. Overall, under certain conditions, surprisingly high  $k_L a$  values of  $>100 \text{ 1/h}$  were found. This seems to be a reason why the OSR50 can support cell densities of  $20 \times 10^6$  cells  $\text{mL}^{-1}$  or more by passive aeration with air. The CFD methods described here can be extended to other OSRs and have the potential to be of value for predicting volumetric scale-up in OSRs.

## Acknowledgments

The authors thank the China Scholarship Council (CSC) and EPFL for financial support (Certification No. 201306120128).

## Notation

- $A$  = interfacial area ( $\text{m}^2$ )
- $a$  = specific interfacial area ( $1/\text{m}$ )
- $C_L^*$  = oxygen saturation concentration in liquid ( $\text{mg/L}$ )
- $d$  = vessel diameter ( $\text{m}$ )
- $D_L$  = diffusion coefficient of gas in liquid ( $\text{m}^2/\text{h}$ )
- $F$  = surface tension ( $\text{kg}/\text{m}^2 \cdot \text{s}^2$ )
- $F_r$  = Froude number
- $g$  = gravity acceleration ( $\text{m}/\text{s}^2$ )
- $H$  = wave height ( $\text{m}$ )
- $k$  = turbulent kinetic energy ( $\text{m}^2/\text{s}^2$ )
- $k_L$  = mass transfer coefficient ( $\text{m/h}$ )
- $n$  = unit normal vector on the interface
- $N$  = shaking speed ( $\text{rpm}$ )
- $p$  = pressure ( $\text{Pa}$ )
- $Re$  = Reynolds number
- $R_S$  = shaking radius ( $\text{m}$ )
- $s$  = surface renewal rate ( $1/\text{s}$ )
- $t$  = time ( $\text{s}$ )
- $t_e$  = exposure time ( $\text{s}$ )
- $u$  = vector of velocity ( $\text{m/s}$ )
- $\bar{u}_z$  = average velocity on  $z$  direction ( $\text{m/s}$ )
- $V_L$  = filling volume ( $\text{m}^3$ )

## Greek letters

- $\alpha$  = volume fraction
- $\alpha_k$  = the Prandtl number for turbulent kinetic energy
- $\alpha_\epsilon$  = the Prandtl number for turbulent dissipation rate
- $\epsilon$  = turbulent dissipation rate ( $\text{m}^2/\text{s}^3$ )
- $\kappa$  = surface curvature ( $1/\text{m}$ )
- $\mu$  = dynamic viscosity ( $\text{kg}/\text{m} \cdot \text{s}^2$ )
- $\mu_{\text{eff}}$  = turbulent viscosity ( $\text{pa} \cdot \text{s}$ )

$\rho$  = density (kg/s<sup>3</sup>)

$\sigma$  = surface tension coefficient (N/m)

$\nu$  = kinematic viscosity (m<sup>2</sup>/s)

$\omega$  = shaking angular velocity (rad/s)

### Subscripts

$g$  = gas phase

$l$  = liquid phase

### Literature Cited

- Eibl R, Kaiser S, Lombriser R, Eibl D. Disposable bioreactors: the current state-of-the-art and recommended applications in biotechnology. *Appl Microbiol Biotechnol.* 2010;86:41–49.
- Muller N, Girard P, Hacker DL, Jordan M, Wurm FM. Orbital shaker technology for the cultivation of mammalian cells in suspension. *Biotechnol Bioeng.* 2005;89:400–406.
- Klößner W, Büchs J. Advances in shaking technologies. *Trends Biotechnol.* 2012;30:307–314.
- Klößner W, Diederichs S, Büchs J. Orbitally shaken single-use bioreactors. *Adv Biochem Eng Biotechnol.* 2014;138:45–60.
- Zhang X, Stettler M, De Sanctis D, Perrone M, Parolini N, Discacciati M, D, Jesus M, Hacker D, Quarteroni A, Wurm FM. Use of orbital shaken disposable bioreactors for mammalian cell cultures from the milliliter-scale to the 1,000-liter scale. *Adv Biochem Eng Biotechnol.* 2009;115:33–53.
- Strnad J, Brinc M, Spudic V, Jelnicar N, Mirnik L, Carman B, Kravanja Z. Optimization of cultivation conditions in spin tubes for Chinese hamster ovary cells producing erythropoietin and the comparison of glycosylation patterns in different cultivation vessels. *Biotechnol Prog.* 2010;26:653–663.
- Monteil DT, Tontodonati G, Ghimire S, Baldi L, Hacker DL, Bürki CA, Wurm FM. Disposable 600-mL orbitally shaken bioreactor for mammalian cell cultivation in suspension. *Biochem Eng J.* 2013;76:6–12.
- Klößner W, Lattermann C, Pursche F, Büchs J, Werner S, Eibl D. Time efficient way to calculate oxygen transfer areas and power input in cylindrical disposable shaken bioreactors. *Biotechnol Prog.* 2014;30:1441–1456.
- Raven N, Rasche S, Kuehn C, Anderlei T, Klößner W, Schuster F, Henquet M, Bosch D, Büchs J, Fischer R, Schillberg S. Scaled-up manufacturing of recombinant antibodies produced by plant cells in a 200-L orbitally-shaken disposable bioreactor. *Biotechnol Bioeng.* 2015;112:308–321.
- Monteil DT, Shen X, Tontodonati G, Baldi L, Hacker DL, Wurm FM. Disposable orbitally shaken TubeSpin bioreactor 600 for Sf9 cell cultivation in suspension. *Anal Biochem.* 2016; 505:26–28.
- De Jesus MJ, Girard P, Bourgeois M, Baumgartner G, Jacko B, Amstutz H, Wurm FM. TubeSpin satellites: a fast track approach for process development with animal cells using shaking technology. *Biochem Eng J.* 2004;17:217–223.
- Xie Q, Michel PO, Baldi L, Hacker DL, Zhang X, Wurm FM. TubeSpin bioreactor 50 for the high-density cultivation of Sf-9 insect cells in suspension. *Biotechnol Lett.* 2011;33:897–902.
- Shen X, Hacker DL, Baldi L, Wurm FM. Virus-free transient protein production in Sf9 cells. *J Biotechnol.* 2014;171:61–70.
- Felix GG, Gomez E. Bioreactor scale-up and oxygen transfer rate in microbial processes: an overview. *Biotechnol Adv.* 2009; 27:153–176.
- Xing ZZ, Kenty BM, Li ZJ, Lee SS. Scale-up analysis for a CHO cell culture process in large-scale bioreactors. *Biotechnol Bioeng.* 2009;103:733–746.
- Löffelholz C, Husemann U, Greller G, Meusel W, Kauling J, Ay P, Kraume M, Eibl R, Eibl D. Bioengineering parameters for single-use bioreactors: overview and evaluation of suitable methods. *Chemie Ingenieur Technik.* 2013;85:40–56.
- Rathore AS, Sharma C, Persad A. Use of computational fluid dynamics as a tool for establishing process design space for mixing in a bioreactor. *Biotechnol Prog.* 2012;28:382–391.
- Sarkar J, Shekhawat LK, Loomba V, Rathore AS. CFD of mixing of multi-phase flow in a bioreactor using population balance model. *Biotechnol Bioeng.* 2016;32:613–628.
- Matasci M, Baldi L, Hacker DL, Wurm FM. The PiggyBac transposon enhances the frequency of CHO stable cell line generation and yields recombinant lines with superior productivity and stability. *Biotechnol Bioeng.* 2011;108:2141–2150.
- Hirt CW, Nichols BD. Volume of fluid (VOF) method for the dynamics of free boundaries. *J Comput Phys.* 1981;39:201–225.
- Brackbill JU, Kothe DB, Zemach C. A continuum method for modeling surface tension. *J Comput Phys.* 1992;100:335–354.
- Schwarze R, Obermeier F. Performance and limitations of the unsteady RANS approach. *Pamm.* 2006;6:543–544.
- Li C, Xia JY, Chu J, Wang YH, Zhuang YP, Zhang SL. CFD analysis of the turbulent flow in baffled shake flasks. *Biochem Eng J.* 2013;70:140–150.
- Büchs J, Maier U, Lotter S, Peter CP. Calculating liquid distribution in shake flasks on rotary shakers at waterlike viscosities. *Biochem Eng J.* 2007;34:200–208.
- Higbie R. The rate of absorption of a pure gas into a still liquid during short periods of exposure. *Trans Am Inst Chem Eng.* 1935;31:365–389.
- Dankwerts PV. Significance of liquid-film coefficients in gas absorption. *Ind Eng Chem.* 1951;43:1460–1467.
- Zhang Z, Thomas CR. Eddy Number distribution in isotropic turbulence and its application for estimating mass transfer coefficients. *Chem Eng Commun.* 1995;140:207–217.
- Running JA, Bansal K. Oxygen transfer rates in shaken culture vessels from fembach flasks to microtiter plates. *Biotechnol Bioeng.* 2016;113:1729–1735.
- Lopes M, Mota M, Belo I. Oxygen mass transfer rate in a pressurized lab-scale stirred bioreactor. *Chem Eng Technol.* 2013; 10:1779–1784.
- Liu T, Miura S, Yaguchi M, Arimura T, Park EY, Okabe M. Scale-up of l-lactic acid production by mutant strain *Rhizopus* sp. MK-96-1196 from 0.003 m<sup>3</sup> to 5 m<sup>3</sup> in airlift bioreactors. *J Biosci Bioeng.* 2006;101:9–12.
- Maier U, Büchs J. Characterisation of the gas-liquid mass transfer in shaking bioreactors. *Biochem Eng J.* 2001;7:99–106.
- Reclari M, Dreyer M, Tissot S, Obreschkow D, Wurm FM, Farhat M. Surface wave dynamics in orbital shaken cylindrical containers. *Phys Fluids.* 2014;26:052104.
- Büchs J, Maier U, Milbradt C, Zoels B. Power consumption in shaking flasks on rotary shaking machines: I. Power consumption measurement in unbaffled flasks at low liquid viscosity. *Biotechnol Bioeng.* 2000;68:589–593.
- Buyevich YA. Particulate stresses in dense disperse flow. *Ind Eng Chem Res.* 1999;38:731–743.
- Hammond TG, Hammond JM. Optimized suspension culture: the rotating-wall vessel. *Am J Physiol Renal Physiol.* 2001;281: 12–25.

Manuscript received May 30, 2016, and revision received Sep. 28, 2016.